STRUCTURAL BIOLOGY COMMUNICATIONS

ISSN 2053-230X

The structure and activity of the glutathione reductase from *Streptococcus pneumoniae*

Mwilye Sikanyika,[a] David Aragão,[b] Christopher A. McDevitt[c] and Megan J. Maher[a]*

[a]Department of Biochemistry and Genetics, La Trobe Institute for Molecular Science, La Trobe University, Melbourne 3086, Australia, [b]Australian Synchrotron, Australian Nuclear Science and Technology Organisation, 800 Blackburn Road, Clayton, Victoria 3168, Australia, and [c]Department of Microbiology and Immunology, Peter Doherty Institute for Infection and Immunity, Melbourne, Victoria 3000, Australia. *Correspondence e-mail: m.maher@latrobe.edu.au

Received 2 July 2018
Accepted 20 November 2018

Edited by C. S. Bond, University of Western Australia, Crawley, Australia

Keywords: glutathione reductase; X-ray crystallography; *Streptococcus pneumoniae*.

PDB reference: glutathione reductase from *Streptococcus pneumoniae*, 6du7

Supporting information: this article has supporting information at journals.iucr.org/f

The glutathione reductase (GR) from *Streptococcus pneumoniae* is a flavoenzyme that catalyzes the reduction of oxidized glutathione (GSSG) to its reduced form (GSH) in the cytoplasm of this bacterium. The maintenance of an intracellular pool of GSH is critical for the detoxification of reactive oxygen and nitrogen species and for intracellular metal tolerance to ions such as zinc. Here, *S. pneumoniae* GR (*Sp*GR) was overexpressed and purified and its crystal structure determined at 2.56 Å resolution. *Sp*GR shows overall structural similarity to other characterized GRs, with a dimeric structure that includes an antiparallel β-sheet at the dimer interface. This observation, in conjunction with comparisons with the interface structures of other GR enzymes, allows the classification of these enzymes into three classes. Analyses of the kinetic properties of *Sp*GR revealed a significantly higher value for $K_{m(GSSG)}$ (231.2 ± 24.7 µ*M*) in comparison to other characterized GR enzymes.

1. Introduction

Glutathione (γ-glutamylcysteinyl-glycine) is a thiol-containing tripeptide that is present at high concentrations (1–10 m*M*) in eukaryotic and many prokaryotic species (Masip *et al.*, 2006). Glutathione can exist in a thiol-reduced state (GSH) or in an oxidized state (GSSG), which consists of two GSH molecules linked together by a disulfide bond. GSH serves as a reductive cofactor for the antioxidant glutaredoxin enzymes (Ritz & Beckwith, 2001), with this activity converting glutathione from the reduced to the oxidized form. The ratio of GSH to GSSG in the bacterial cytoplasm is tightly regulated by the enzyme glutathione reductase (GR), which employs NADPH as the electron donor:

$$\mathrm{GSSG} + \mathrm{NADPH} + \mathrm{H^+} \rightarrow \mathrm{NADP^+} + 2\mathrm{GSH}. \qquad (1)$$

The Gram-positive bacterium *Streptococcus pneumoniae* (the pneumococcus) is the world's foremost human bacterial pathogen. It is the leading cause of bacterial pneumonia, which accounts for 15% of all childhood disease mortality (Rudan *et al.*, 2008, 2013). The acquisition of nutrients is essential to the ability of the pneumococcus to colonize and to mediate *in vivo* virulence. Analyses of genome sequences have revealed that *S. pneumoniae* lacks the genes required for *de novo* glutathione biosynthesis (Lanie *et al.*, 2007). Instead, *S. pneumoniae* acquires GSH (~10.9 ± 0.3 m*M*) from the extracellular environment via an ATP-binding cassette (ABC) transporter and the substrate-binding protein GshT (Potter *et al.*, 2012; Begg *et al.*, 2015). Isogenic deletion strains lacking either *gshT* or *gor*, which encodes GR, showed increased sensitivity to oxidative stress, albeit to differing extents (Potter

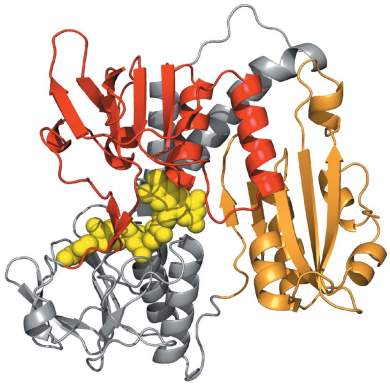

et al., 2012). Further, the Δ*gshT* and Δ*gor* strains were observed to be hypersensitive to intoxication by the divalent metal ions copper, zinc and cadmium (Potter *et al.*, 2012; Begg *et al.*, 2015).

Murine models of invasive pneumococcal infection have observed that infection triggers an innate immune response that includes increased levels of reactive oxygen and nitrogen species (ROS/RNS) and significant fluxes in the abundance of host metal ions such as zinc (Zn^{2+}; McDevitt *et al.*, 2011). This latter observation has been implicated in potentially exposing invading bacteria to zinc stress either directly or as a component of phagocytic cell killing (Botella *et al.*, 2011; Martin *et al.*, 2017; Eijkelkamp *et al.*, 2014). Glutathione has been implicated in playing crucial roles in protection against these host-mediated stresses. ROS and RNS can be detoxified by GSH via direct interaction or by enzymatic processes, such as that catalyzed by glutathione peroxidase. Glutathione also forms metal complexes and thereby can contribute to the intracellular metal tolerance of ions such as zinc by forming a GSH–Zn^{2+} complex to moderate the abundance of the uncomplexed ion (Díaz-Cruz *et al.*, 1998). These protective processes are dependent on cytoplasmic GSH, the concentration of which is dictated by *S. pneumoniae* GR.

The crystal structures of GR enzymes from *Escherichia coli* (Mittl & Schulz, 1994), *Saccharomyces cerevisiae* (Yu & Zhou, 2007), *Plasmodium falciparum* (Sarma *et al.*, 2003; Böhme *et al.*, 2000) and *Homo sapiens* (Schulz *et al.*, 1978; Karplus & Schulz, 1989; Savvides & Karplus, 1996; Berkholz *et al.*, 2008) have been described in conjunction with their kinetic properties (Mittl & Schulz, 1994; Savvides & Karplus, 1996; Yu & Zhou, 2007). All three enzymes are dimeric and bind one molecule of FAD per subunit. Here, we report the structural and kinetic characterization of the GR enzyme from *S. pneumoniae* (*Sp*GR). Comparison of the *Sp*GR structure with those from other sources reveals close similarities in the overall structures of these enzymes, with secondary-structural differences apparent at the dimer interface.

2. Materials and methods

2.1. Macromolecule production

Recombinant *Sp*GR was generated by PCR-amplification of the SPD_0685 gene from *S. pneumoniae* serotype 2 strain D39 using ligation-independent cloning and the oligonucleotides GR_LIC1F (5′-TGGGTGGTGGATTTCCTAGAGAA TATGATATCATTGCTATCGG) and GR_LIC1R (5′-TTG GAAGTATAAATTTCCACGCATGGTTACAAATTCTTC) to insert the gene into an N-terminal dodecahistidine tag-containing vector, pCAMnLIC01, to generate pCAMnLIC01-GR.

Heterologous expression of recombinant *Sp*GR was performed in *E. coli* BL21(DE3) cells grown in lysogeny broth at 37°C. The expression of recombinant protein was induced by 0.5 m*M* IPTG at an optical density (OD) of 0.6. The cells were incubated at 25°C for 20 h and were then harvested by high-speed centrifugation. The cell pellet was suspended in buffer *A* (20 m*M* Tris pH 7.5, 150 m*M* NaCl) and disrupted using a TS series benchtop cell disruptor (Constant Systems). The His-tagged *Sp*GR protein was purified using a two-step protocol consisting of immobilized metal-affinity chromatography (IMAC) followed by size-exclusion chromatography. The cell lysate was applied onto Ni-Sepharose 6 Fast Flow resin (GE Healthcare Life Sciences) equilibrated with buffer *A* and eluted with buffer *A* containing 300 m*M* imidazole. The eluted *Sp*GR protein was incubated with 2 m*M* FAD for 2 h at 4°C before application onto a HiLoad 16/600 Superdex 200 size-exclusion column (GE Healthcare Life Sciences) pre-equilibrated with buffer *A*. The purified *Sp*GR protein was concentrated to ∼20 mg ml^{-1} as determined by a BCA assay (ThermoFisher Scientific) and was stored at −80°C until further use. Macromolecule-production information is summarized in Table 1.

Table 1
Macromolecule-production information.

Source organism	*S. pneumoniae*
DNA source	*S. pneumoniae* serotype 2 strain D39
Forward primer	TGGGTGGTGGATTTCCTAGAGAATATGATA TCATTGCTATCGG
Reverse primer	TTGGAAGTATAAATTTCCACGCATGGTTAC AAATTCTTC
Expression vector	pCAMnLIC01
Expression host	*E. coli* strain BL21(DE3)
Complete amino-acid sequence of the construct produced	MREYDIIAIGGGSGGIATMNRAGEHGAQAA VIEEKKLGGTCVNVGCVPKKIMWYGAQI AETFHQFGEDYGFKTTDLNFDFATLRRN RESYIDRARSSYDGSFKRNGVDLIEGHA EFVDSHTVSVNGELIRAKHIVIATGAHP SIPNIPGAELGGSSDDVFAWEELPESVA ILGAGYIAVELAGVLHTFGVKTDLFVRR DRPLRGFDSYIVEGLVKEMERTNLPLHT HKVPVKLEKTTDGITIHFEDGTSHTASQ VIWATGRRPNVKGLQLEKAGVTLNERGF IQVDEYQNTVVEGIYALGDVTGEKELTP VAIKAGRTLSERLFNGKTTAKMDYSTIP TVVFSHPAIGTVGLTEEQAIKEYGQDQI KVYKSSFASMYSACTRNRQESRFKLITA GSEEKVVGLHGIGYGVDEMIQGFAVAIK MGATKADFDATVAIHPTSSEEFVTMR

2.2. Crystallization

Initial crystallization trials were carried out with commercially available screens (Molecular Dimensions and Qiagen) by the sitting-drop vapour-diffusion method using equal volumes (0.2 µl) of protein sample (10–20 mg ml^{-1} in 20 m*M* Tris, 0.15 *M* NaCl pH 7.5) and reservoir solution dispensed using a Crystal Gryphon robot (Art Robbins Instruments). Initial crystals grew after four weeks in 0.2 *M* potassium thiocyanate, 0.1 *M* bis-Tris propane pH 7.5, 20%(*w*/*v*) PEG 3350. Optimization of this condition yielded crystals of approximate dimensions 50 × 150 × 150 µm that were grown by hanging-drop vapour diffusion at 20°C by mixing equal volumes (1 µl) of protein solution (20 mg ml^{-1} in 20 m*M* Tris, 0.15 *M* NaCl pH 7.5) and reservoir solution (0.1 *M* bis-Tris propane pH 7.0, 0.2 *M* potassium thiocyanate, 14% PEG 3350, 0.1 m*M* $NADP^+$) and equilibrating the drops against 0.5 ml reservoir solution. A single *Sp*GR crystal was transferred to cryoprotectant solution (0.1 *M* bis-Tris propane pH 7.0, 0.2 *M*

Table 2
Crystallization.

Method	Hanging drop
Plate type	VDXm plates
Temperature (K)	293
Protein concentration (mg ml^{-1})	16
Buffer composition of protein solution	20 m*M* Tris–HCl pH 7.5, 150 m*M* NaCl
Composition of reservoir solution	0.2 *M* potassium thiocyanate, 0.1 *M* bis-Tris propane pH 7.0, 14%(*w*/*v*) PEG 3350, 0.1 m*M* NADP$^+$
Volume and ratio of drop	2 µl, 1:1
Volume of reservoir (µl)	500

Table 3
Data collection and processing.

Values in parentheses are for the outer shell.

Diffraction source	MX2 beamline, Australian Synchrotron (Aragão *et al.*, 2018)
Wavelength (Å)	0.954
Temperature (K)	100
Detector	ADSC Quantum 315r
Crystal-to-detector distance (mm)	400
Rotation range per image (°)	0.5
Total rotation range (°)	180
Exposure time per image (s)	0.5
Space group	$P2_1$
a, *b*, *c* (Å)	96.75, 172.67, 135.43
α, β, γ (°)	90, 91.05, 90
Mosaicity (°)	0.21
Resolution range (Å)	50–2.56 (2.60–2.56)
Total No. of reflections	531768
No. of unique reflections	141364
Completeness (%)	98.9 (84.1)
Multiplicity	3.8 (3.4)
$\langle I/\sigma(I)\rangle$	8.7 (1.5)
$R_{\rm p.i.m.}$ (%)	6.2 (39.0)
$CC_{1/2}$	0.994 (0.641)
Overall *B* factor from Wilson plot (Å^2)	39.3

potassium thiocyanate, 14% PEG 3350, 0.1 m*M* NADP$^+$, 21% glucose) and flash-cooled in liquid nitrogen. Crystallization information is summarized in Table 2.

2.3. Data collection and processing

Diffraction data were recorded on an ADSC Quantum 315r detector at 100 K (in a nitrogen stream) on beamline MX2 at the Australian Synchrotron at a wavelength of 0.954 Å. Data were processed with *XDS* (Kabsch, 2010) and were merged and scaled with *AIMLESS* (Evans & Murshudov, 2013). Data-collection and processing statistics are summarized in Table 3

2.4. Structure solution and refinement

The structure of *Sp*GR was solved by molecular replacement with *Phaser* (McCoy *et al.*, 2007). A search model was generated with *CHAINSAW* (Stein, 2008) from the structure of *E. coli* GR (*Ec*GR; 61% sequence identity; PDB entry 1ger; Mittl & Schulz, 1994). Refinement was carried out using *REFMAC*5 (Murshudov *et al.*, 2011) with iterative cycles of model building in *Coot* (Emsley & Cowtan, 2004). Tight noncrystallographic symmetry (NCS) restraints were applied during the early stages of refinement. These were relaxed and removed entirely as refinement progressed. Model geometry was analysed by *MolProbity* (Chen *et al.*, 2010). Refinement statistics are summarized in Table 4.

Table 4
Structure solution and refinement.

Values in parentheses are for the outer shell.

Resolution range (Å)	50–2.56 (2.62–2.56)
Completeness (%)	98.7
σ Cutoff	None
No. of reflections, working set	134126 (8684)
No. of reflections, test set	7170 (434)
Final $R_{\rm cryst}$	0.180 (0.326)
Final $R_{\rm free}$	0.233 (0.338)
Cruickshank DPI	0.229
No. of non-H atoms	
Protein	27516
Ligand	430
Solvent	1766
Total	29712
R.m.s. deviations	
Bond lengths (Å)	0.007
Angles (°)	1.079
Average *B* factor (Å^2)	43.34
Ramachandran plot	
Most favoured (%)	96.8
Allowed (%)	99.7
PDB code	6du7

3. Results and discussion

3.1. Overall structure of *Sp*GR

*Sp*GR crystallized in space group $P2_1$ with eight molecules in the asymmetric unit (arranged as four homodimers; Fig. 2*b*). All residues (1–448) were modelled in chains *A*, *B*, *C*, *D*, *F* and *G*, while chains *E* and *H* included 447 and 446 residues, respectively. Refinement of the model to 2.56 Å resolution converged with residuals of R = 18.0% and $R_{\rm free}$ = 23.3% with excellent statistics and model geometry. The atomic coordinates and structure factors have been deposited in the Protein Data Bank (PDB) with accession code 6du7 (Table 4).

The observation of dimeric *Sp*GR assemblies in the crystal is consistent with the analysis of the purified protein by size-exclusion chromatography (Fig. 1), which showed that *Sp*GR eluted at an elution volume corresponding to a molecular weight of approximately 100 kDa. These data confirm that *Sp*GR was also present as a dimer in solution (Fig. 1) and are consistent with the structural characterization of GR enzymes from *E. coli* (*Ec*GR; Mittl & Schulz, 1994), *H. sapiens* (*h*GR; Schulz *et al.*, 1978; Karplus & Schulz, 1989; Savvides & Karplus, 1996; Berkholz *et al.*, 2008), *P. falciparum* (*Pf*GR; Sarma *et al.*, 2003; Böhme *et al.*, 2000) and *S. cerevisiae* (*y*GR; Yu & Zhou, 2007). There are no significant differences between the backbone structures of the eight molecules in the asymmetric unit, as shown by r.m.s.d. values ranging from 0.2 to 0.4 Å for the superposition of 446 common C^α atoms between each combination of monomer pairs.

The *Sp*GR monomer consists of three distinct domains: an NADPH-binding domain (residues 139–263), an FAD-binding domain (residues 1–138 and 264–334) and a dimerization domain (residues 335–448) (Fig. 2*a*). The NADPH-binding and FAD-binding domains both show Rossmann folds, and the

Table 5
Structural comparisons between *Sp*GR and homologues.

Organism	PDB code	R.m.s.d. (Å)	N_{align}	Sequence identity (%)
Vibrio parahaemolyticus	5u1o	0.74	444	59
Streptococcus mutans	5v36	0.95	441	60
Escherichia coli	1ger	0.94	445	61
Homo sapiens	1gra	1.23	444	51
Yersinia pestis	5vdn	0.95	444	59
Plasmodium falciparum	1onf	1.11	425	44
Saccharomyces cerevisiae	2hqm	1.06	436	47
Chromatium gracile†	2r9z	1.21	437	49

† Glutathione amide reductase (Van Petegem *et al.*, 2007).

dimerization domain comprises five α-helices and five β-strands. GR enzymes contain a redox-active disulfide bond that is reduced by NADPH via FAD (Pai & Schulz, 1983), which is observed between residues Cys41 and Cys46 in the *Sp*GR structure, and is positioned adjacent to the isoalloxazine ring of the FAD cofactor. The FAD cofactor is bound in an extended conformation within the FAD-binding domain.

The *Sp*GR coordinates were used to perform a secondary-structure search of the PDB with *PDBeFold* (http://www.ebi.ac.uk/msd-srv/ssm; Krissinel & Henrick, 2004) and revealed close structural similarities between the *Sp*GR structure and those of *Ec*GR, *h*GR, *y*GR and *Pf*GR, in addition to those of the GR enzymes from *Vibrio parahaemolyticus* (*Vp*GR; PDB entry 5u1o), *Yersinia pestis* (*Yp*GR; PDB entry 5vdn) and *S. mutans* (*Sm*GR; PDB entry 5v36), all of which are unpublished (Table 5). In addition, the *Sp*GR structure is closely similar to that of the glutathione amide reductase from *Chromatium gracile* (Table 5; Van Petegem *et al.*, 2007).

3.2. Structure of the subunit interface

The subunit interface of *Sp*GR shows a total buried surface area of 3502 Å^2 per monomer, comprising ∼16% of the surface area of each protomer. Two main structural regions contribute to dimer formation: residues 46–93 from the

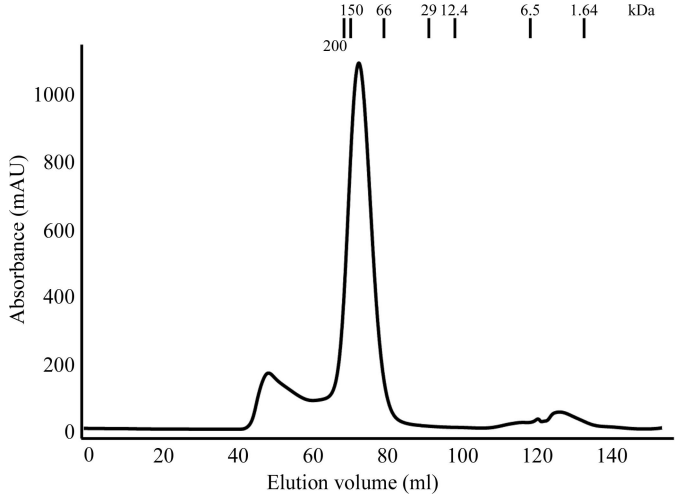

Figure 1
Purification of *Sp*GR. The elution profile of purified *Sp*GR relative to the indicated protein standards analysed by size-exclusion chromatography. The molecular weight of the *Sp*GR protein is estimated to be 100 kDa, which corresponds to a homodimer.

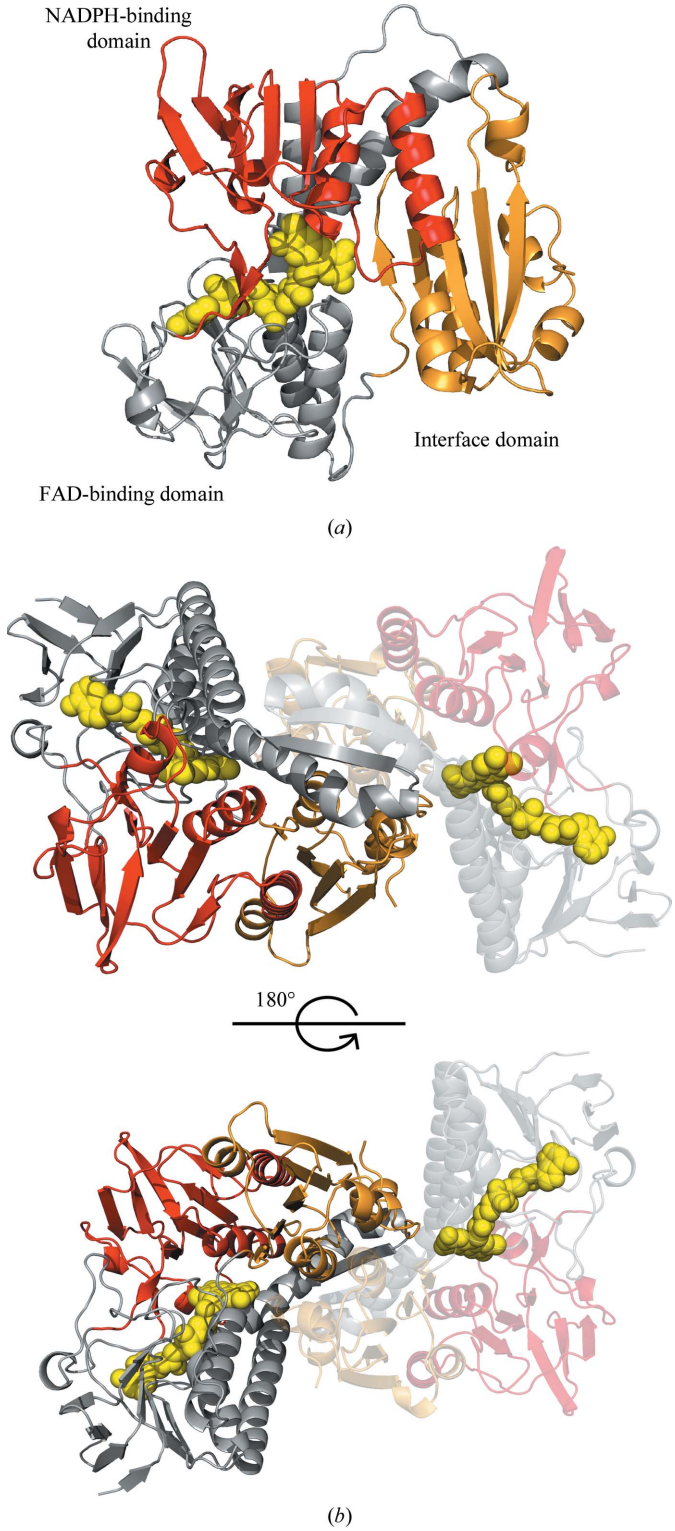

Figure 2
Structure of the glutathione reductase from *S. pneumoniae*. (*a*) The structure of the *Sp*GR monomer is shown in cartoon representation with the FAD-binding domain in grey, the NADPH-binding domain in red and the interface domain in gold. The FAD cofactor is represented as yellow spheres. (*b*) Structure of the *Sp*GR dimer: both monomers are coloured according to their domain structures as in (*a*).

FAD-binding domain (buried surface area of 1276 Å^2) and residues 408–448 at the C-terminus of the dimerization domain (buried surface area of 1481 Å^2).

Residues 70–79 from each monomer align at the dimer interface in an antiparallel β-sheet structure (Fig. 3). This closely mirrors the structure of the dimerization interface of *Ec*GR, but is distinct from those observed for *y*GR and *h*GR.

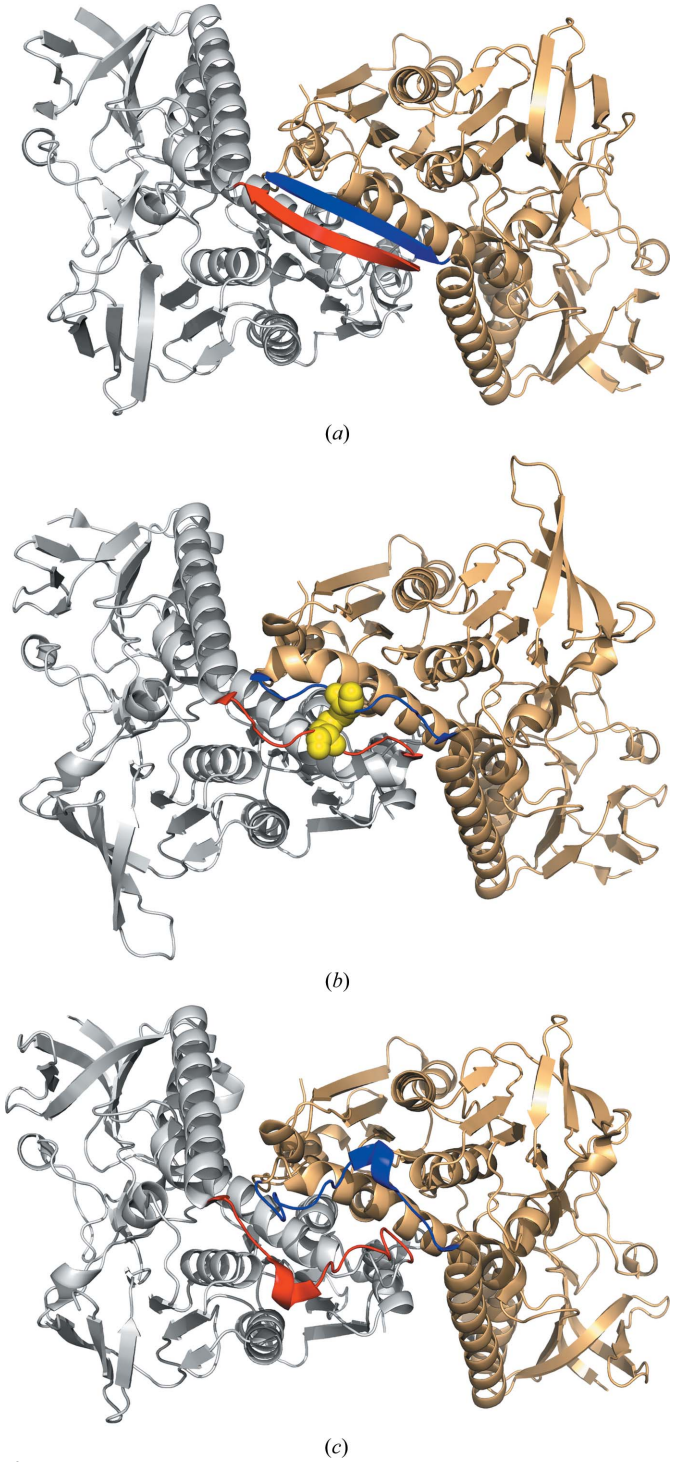

Figure 3
The structures of the dimer interfaces for GR enzymes (highlighted in red and blue). (*a*) *Sp*GR (this work), (*b*) *h*GR (PDB entry 3dk4), (*c*) *y*GR (PDB entry 2hqm).

In *h*GR an intersubunit disulfide bridge between residues Cys90 and Cys90′ is present in this position, while the *y*GR structure features a short α-helix connected by two loose loops owing to an insertion of six residues in this region of the structure (Fig. 3). The determination of the *Sp*GR structure described here divides GR enzymes into three classes based on the structures of the dimer interfaces (Fig. 3). These are disulfide-linked (*h*GR), looped (*y*GR) and β-sheet (*Ec*GR, *Sp*GR, *Pf*GR and other bacterial homologues). The bacterial enzymes therefore represent the major class (as defined by the structures of their dimer interfaces), all of which share the same structural features in this region (Fig. 3). Despite these structural differences, the composition of the GR dimer interface does not appear to determine the enzyme activity. Mutagenesis of the *Ec*GR protein to introduce an intersubunit disulfide bond, similar to that observed in the *h*GR enzyme, did not have an impact on its catalytic activity or thermal stability (Scrutton *et al.*, 1988).

The catalytic mechanism and the location of the substrate-binding sites in *h*GR have been extensively investigated through X-ray crystallographic analyses of crystals soaked with NADPH and glutathione (Karplus & Schulz, 1989). A comparison of the *Sp*GR structure with that of *h*GR shows that the dimer interface contributes to the structure of the GSSG binding pocket, which is composed of residues from both monomers. The binding pocket for NADPH is separated from the GSSG binding site by the Cys41–Cys46 disulfide linkage. Despite the fact that the *Sp*GR crystallization conditions contained NADP$^+$, we did not observe evidence for bound NADP$^+$ in the electron density. The presence of the disulfide linkage in the *Sp*GR structure described here confirms that this structure was solved in the oxidized (resting) state. Extensive analyses of the activities of GR enzymes from other sources have demonstrated the importance of this linkage in enzyme catalysis, where it mediates hydride transfer from NADPH to GSSG (Karplus & Schulz, 1989).

3.3. Kinetic analyses of the *Sp*GR enzyme

Michaelis–Menten analyses of the glutathione reductase activity of *Sp*GR for the substrates NADPH and GSSG revealed the kinetic parameters $K_{m(NADPH)}$ = 23.2 ± 3.3 µ*M*, $K_{m(GSSG)}$ = 231.2 ± 24.7 µ*M* and V_{max} = 319.3 ± 15.9 µmol min^{-1} mg^{-1} (Table 6). The values of V_{max} and $K_{m(NADPH)}$ for *Sp*GR are consistent with those for the other characterized enzymes in this family; however, the determined value of $K_{m(GSSG)}$ for *Sp*GR is significantly higher than those reported for the majority of kinetically characterized GRs (Table 6). The only exception is the GR enzyme from spinach, which has a comparable $K_{m(GSSG)}$ to that of *Sp*GR.

Although we were unable to determine the structure of the *Sp*GR enzyme in the presence of the substrates NADPH and GSSG, we predicted the binding locations of these molecules by superposition with the structure of *h*GR, which has been solved in complex with NADP$^+$ and GSSG (PDB entry 3dk4; Berkholz *et al.*, 2008). We observed that the structures of the respective NADPH and GSSG binding sites are almost

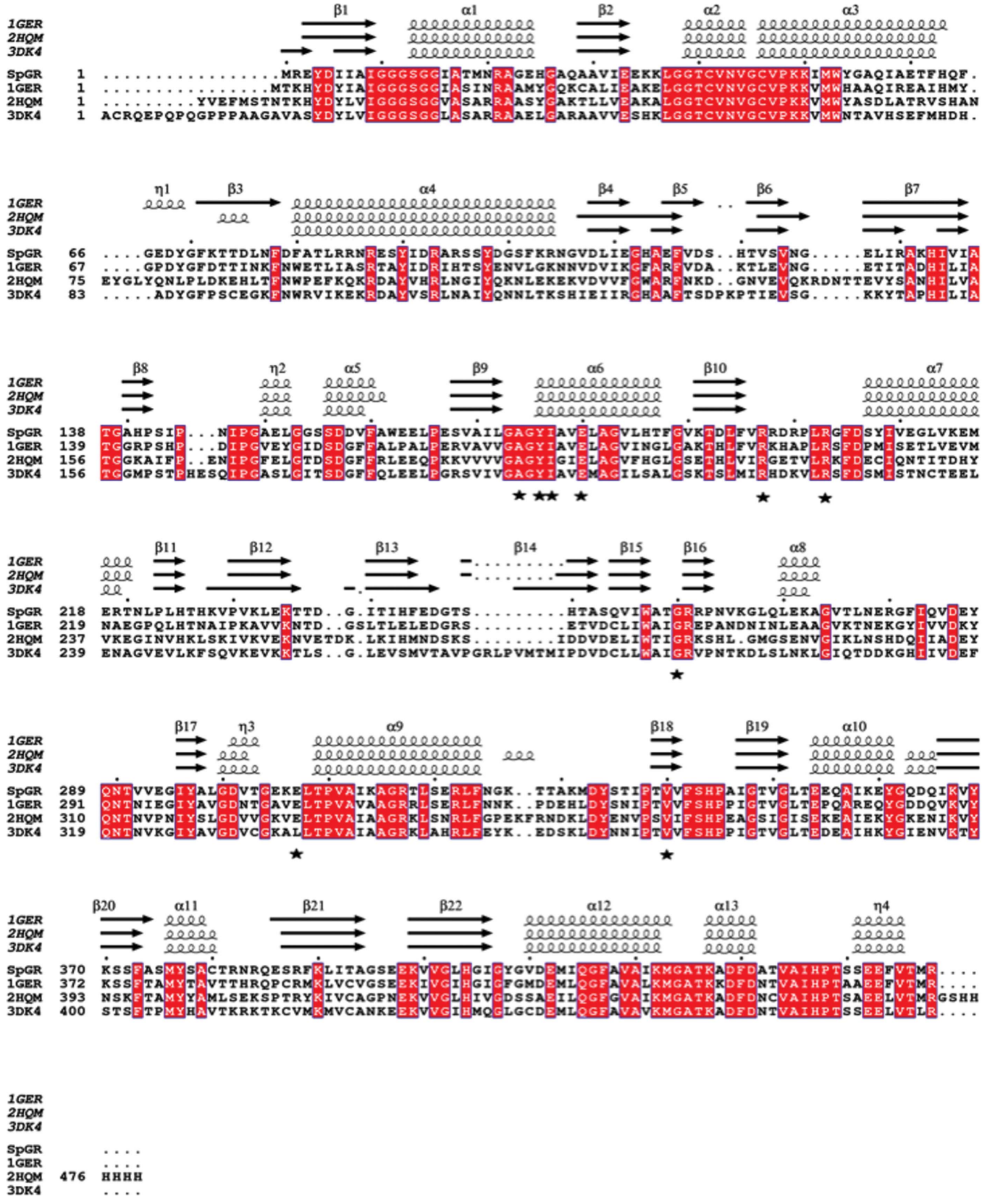

Figure 4
Sequence alignment of *Sp*GR against the *Ec*GR, *h*GR and *y*GR homologues. The alignment was performed using *T-Coffee* and *ESPript* (http://tcoffee.crg.cat/apps/tcoffee/do:expresso; Robert & Gouet, 2014). The secondary-structural elements were identified from PDB entries 1ger, 2hqm and 3dk4 using *ESPript* and are displayed at the top of the alignment. The α-helices and β-sheets are denoted α and β, respectively. Conserved residues are indicated by white lettering on a red background. Resides that form the NADPH-binding site are indicated with black stars.

Table 6
Kinetic parameters for GR enzymes from various organisms.

Organism	V_{max} (μmol min^{-1} mg^{-1})	$K_{m(NADPH)}$ (μ*M*)	$K_{m(GSSG)}$ (μ*M*)
Streptococcus pneumoniae†	319 ± 16	23.2 ± 3.3	231 ± 25
Homo sapiens‡	147§	8.5	65
Escherichia coli¶	360.6§	16	66
Saccharomyces cerevisiae††	166.7§	15	74.6
Plasmodium falciparum‡‡	204§	4.8 ± 0.4	69 ± 2
Calf liver§§	190§	21.1 ± 1	101 ± 7
Rat liver¶¶	207§	8.2 ± 0.8	26.3 ± 5.7
Phaeodactylum tricornutum†††	190§	14	60
Pea‡‡‡	26§	3	62
Spinach§§§	246§	2.78 ± 0.34	196 ± 40

† This work. ‡ Savvides & Karplus (1996), Storey *et al.* (1998). § Errors were not reported. ¶ Mittl & Schulz (1994). †† Yu & Zhou (2007). ‡‡ Böhme *et al.* (2000). §§ Carlberg & Mannervik (1981). ¶¶ Carlberg *et al.* (1981). ††† Arias *et al.* (2010). ‡‡‡ Connell & Mullet (1986). §§§ Halliwell & Foyer (1978).

identical in the *Ec*GR, *h*GR, *y*GR and *Sp*GR enzymes. The *h*GR complex structure defined nine residues that directly interact with the substrate NADPH (Ala195, Tyr197, Ile198, Glu201, Arg218, Arg224, Gly290, Leu337 and Val370; Karplus & Schulz, 1989), eight of which are conserved in the sequences of *Sp*GR, *Ec*GR and *y*GR (Fig. 4). The single substitution is that of Leu337 in *h*GR for Glu in *Sp*GR, *Ec*GR and *y*GR. Based on the kinetic data [$K_{m(NADPH)}$ = 23.2 ± 3.3 μ*M*], this substitution does not appear to affect the affinity of binding of NADPH to *Sp*GR. In the structure of *h*GR in complex with $NADP^+$ and GSSG, the interaction of this residue with the substrate NADPH is side-chain-independent, being mediated by a hydrogen bond between its amide nitrogen and NADPH. The close structural similarities between the GSSG binding sites in the *Sp*GR, *h*GR, *Ec*GR and *y*GR enzymes indicate no obvious features that would explain the differences in the kinetic parameters [specifically $K_{m(GSSG)}$] for these enzymes.

4. Conclusion

The crystal structure of *Sp*GR determined at 2.56 Å resolution shows high structural conservation with GR enzymes from human, *E. coli* (and other bacterial organisms) and *S. cerevisiae*. Despite the significant structural conservation, kinetic studies reveal a weaker affinity of the enzyme for its substrate, GSSG. Further investigation of the links between the structural and kinetic properties of *Sp*GR must await its structure solution in the presence of bound substrates.

Acknowledgements

Aspects of this research were undertaken on the Macromolecular Crystallography beamline MX2 at the Australian Synchrotron, Victoria, Australia and we thank the beamline staff for their enthusiastic and professional support.

Funding information

This work was funded by the National Health and Medical Research Council of Australia (GNT1080784 to MJM, DA and CAM). MS was funded by a La Trobe University Full Fee Research Scholarship (LTUFFRS).

References

Aragão, D., Aishima, J., Cherukuvada, H., Clarken, R., Clift, M., Cowieson, N. P., Ericsson, D. J., Gee, C. L., Macedo, S., Mudie, N., Panjikar, S., Price, J. R., Riboldi-Tunnicliffe, A., Rostan, R., Williamson, R. & Caradoc-Davies, T. T. (2018). *J. Synchrotron Rad.* **25**, 885–891.
Arias, D. G., Marquez, V. E., Beccaria, A. J., Guerrero, S. A. & Iglesias, A. A. (2010). *Protist*, **161**, 91–101.
Begg, S. L., Eijkelkamp, B. A., Luo, Z., Couñago, R. M., Morey, J. R., Maher, M. J., Ong, C. L., McEwan, A. G., Kobe, B., O'Mara, M. L., Paton, J. C. & McDevitt, C. A. (2015). *Nature Commun.* **6**, 6418.
Berkholz, D. S., Faber, H. R., Savvides, S. N. & Karplus, P. A. (2008). *J. Mol. Biol.* **382**, 371–384.
Böhme, C. C., Arscott, L. D., Becker, K., Schirmer, R. H. & Williams, C. H. Jr (2000). *J. Biol. Chem.* **275**, 37317–37323.
Botella, H., Peyron, P., Levillain, F., Poincloux, R., Poquet, Y., Brandli, I., Wang, C., Tailleux, L., Tilleul, S., Charrière, G. M., Waddell, S. J., Foti, M., Lugo-Villarino, G., Gao, Q., Maridonneau-Parini, I., Butcher, P. D., Castagnoli, P. R., Gicquel, B., de Chastellier, C. & Neyrolles, O. (2011). *Cell Host Microbe*, **10**, 248–259.
Carlberg, I., Altmejd, B. & Mannervik, B. (1981). *Biochim. Biophys. Acta*, **677**, 146–152.
Carlberg, I. & Mannervik, B. (1981). *Anal. Biochem.* **116**, 531–536.
Chen, V. B., Arendall, W. B., Headd, J. J., Keedy, D. A., Immormino, R. M., Kapral, G. J., Murray, L. W., Richardson, J. S. & Richardson, D. C. (2010). *Acta Cryst.* D**66**, 12–21.
Connell, J. P. & Mullet, J. E. (1986). *Plant Physiol.* **82**, 351–356.
Díaz-Cruz, M. S., Mendieta, J., Monjonell, A., Tauler, R. & Esteban, M. (1998). *J. Inorg. Biochem.* **70**, 91–98.
Eijkelkamp, B. A., Morey, J. R., Ween, M. P., Ong, C. L., McEwan, A. G., Paton, J. C. & McDevitt, C. A. (2014). *PLoS One*, **9**, e89427.
Emsley, P. & Cowtan, K. (2004). *Acta Cryst.* D**60**, 2126–2132.
Evans, P. R. & Murshudov, G. N. (2013). *Acta Cryst.* D**69**, 1204–1214.
Halliwell, B. & Foyer, C. H. (1978). *Planta*, **139**, 9–17.
Kabsch, W. (2010). *Acta Cryst.* D**66**, 125–132.
Karplus, P. A. & Schulz, G. E. (1989). *J. Mol. Biol.* **210**, 163–180.
Krissinel, E. & Henrick, K. (2004). *Acta Cryst.* D**60**, 2256–2268.
Lanie, J. A., Ng, W.-L., Kazmierczak, K. M., Andrzejewski, T. M., Davidsen, T. M., Wayne, K. J., Tettelin, H., Glass, J. I. & Winkler, M. E. (2007). *J. Bacteriol.* **189**, 38–51.
Martin, J. E., Edmonds, K. A., Bruce, K. E., Campanello, G. C., Eijkelkamp, B. A., Brazel, E. B., McDevitt, C. A., Winkler, M. E. & Giedroc, D. P. (2017). *Mol. Microbiol.* **104**, 636–651.
Masip, L., Veeravalli, K. & Georgiou, G. (2006). *Antioxid. Redox Signal.* **8**, 753–762.
McCoy, A. J., Grosse-Kunstleve, R. W., Adams, P. D., Winn, M. D., Storoni, L. C. & Read, R. J. (2007). *J. Appl. Cryst.* **40**, 658–674.
McDevitt, C. A., Ogunniyi, A. D., Valkov, E., Lawrence, M. C., Kobe, B., McEwan, A. G. & Paton, J. C. (2011). *PLoS Pathog.* **7**, e1002357.
Mittl, P. R. & Schulz, G. E. (1994). *Protein Sci.* **3**, 799–809.
Murshudov, G. N., Skubák, P., Lebedev, A. A., Pannu, N. S., Steiner, R. A., Nicholls, R. A., Winn, M. D., Long, F. & Vagin, A. A. (2011). *Acta Cryst.* D**67**, 355–367.
Pai, E. F. & Schulz, G. E. (1983). *J. Biol. Chem.* **258**, 1752–1757.
Potter, A. J., Trappetti, C. & Paton, J. C. (2012). *J. Bacteriol.* **194**, 6248–6254.
Ritz, D. & Beckwith, J. (2001). *Annu. Rev. Microbiol.* **55**, 21–48.
Robert, X. & Gouet, P. (2014). *Nucleic Acids Res.* **42**, W320–W324.
Rudan, I., Boschi-Pinto, C., Biloglav, Z., Mulholland, K. & Campbell, H. (2008). *Bull. World Health Organ.* **86**, 408–416.

Rudan, I., O'Brien, K. L., Nair, H., Liu, L., Theodoratou, E., Qazi, S., Lukšić, I., Fischer Walker, C. L., Black, R. E. & Campbell, H. (2013). *J. Glob. Health*, **3**, 010401.
Sarma, G. N., Savvides, S. N., Becker, K., Schirmer, M., Schirmer, R. H. & Karplus, P. A. (2003). *J. Mol. Biol.* **328**, 893–907.
Savvides, S. N. & Karplus, P. A. (1996). *J. Biol. Chem.* **271**, 8101–8107.
Schulz, G. E., Schirmer, R. H., Sachsenheimer, W. & Pai, E. F. (1978). *Nature (London)*, **273**, 120–124.
Scrutton, N. S., Berry, A. & Perham, R. N. (1988). *FEBS Lett.* **241**, 46–50.
Stein, N. (2008). *J. Appl. Cryst.* **41**, 641–643.
Storey, B. T., Alvarez, J. G. & Thompson, K. A. (1998). *Mol. Reprod. Dev.* **49**, 400–407.
Van Petegem, F., De Vos, D., Savvides, S., Vergauwen, B. & Van Beeumen, J. (2007). *J. Mol. Biol.* **374**, 883–889.
Yu, J. & Zhou, C.-Z. (2007). *Proteins*, **68**, 972–979.